Journal of Rock Mechanics and Geotechnical Engineering 15 (2023) 2994–3009

Contents lists available at ScienceDirect

Journal of Rock Mechanics and Geotechnical Engineering

journal homepage: www.jrmge.cn

Full Length Article

New semi-analytical approach for ice lens heaving during artificial freezing of fine-grained material

K. Niggemann*, R. Fuentes

Institute of Geomechanics and Underground Technology, RWTH Aachen University, Aachen, Germany

ARTICLE INFO

Article history:
Received 22 October 2022
Received in revised form
8 May 2023
Accepted 9 July 2023
Available online 6 August 2023

Keywords:
Semi-analytical approach
Ice lens formation
Frost heaving
Bottom freezing
Segregation potential
Frost-susceptible soil

ABSTRACT

The calculation of frost heaving with ice lens formation is still not standard for construction projects using artificial ground freezing (AGF). In fine-grained material, ice lenses may initiate and lead to significant heaving at the ground surface, which should be considered in advance. However, the complex processes during ice lens formation are still not fully understood and difficult to capture in a simple approach. In the past, the semi-analytical approach of Konrad and Morgenstern used one soil constant, the "segregation potential (SP)". It has been mainly and most successfully applied to the heave calculation of natural-induced soil freezing in cold regions. Its application to AGF has been so far unsuccessful. To solve this, a new semi-analytical approach is presented in this paper. It includes AGF conditions such as bottom-up freezing, temperature gradients to reach great freezing velocities, and a distinction between two freezing states. One is the freezing-up state until a certain frost body thickness is reached (thermal transient state), and the other is a holding phase where the frost body thickness is kept constant (thermal quasi-steady state). To test its ability, the results are applied to another freezing direction, the top-down freezing. The new approach is validated using two different frost-susceptible soils and, in total, 50 frost heave tests. In the thermal transient region, where the SP is applicable, the two semi-analytical approaches are compared, showing improved performance of the current method by about 15%.
© 2023 Institute of Rock and Soil Mechanics, Chinese Academy of Sciences. Production and hosting by Elsevier B.V. This is an open access article under the CC BY-NC-ND license (http://creativecommons.org/licenses/by-nc-nd/4.0/).

1. Introduction

Artificial ground freezing (AGF) is often used in urban infrastructure projects. The frost body expansion can cause deformation and heaving at the surface, especially in fine-grained soils due to ice lens formation. For construction projects using AGF, a monitoring system to control deformation is essential. The monitoring includes a structural control of the object, the adjacent infrastructure, and the ground surface. Besides monitoring, the ability to model the process is also crucial for control purposes. The prediction of frost heaving with ice lens formation for AGF projects usually is based on soil frost susceptibility recommendations (Auld et al., 2015). However, in most cases, frost heaving is not predicted in practice because practice-oriented calculation methods are missing. An engineer can use numerical methods. Ji et al. (2019) divided numerical models for frost heave calculation into two categories: mechanistic frost heave models and physical field models.

The first group includes models that explain the mechanism of frost heaving and the initiation of discrete ice lenses in the soil during freezing. These models assume a frozen fringe between the ice lens and the freezing front and take into account the interface pressure between water and solid, which leads to the freezing suction (Gilpin, 1980; O'Neill and Miller, 1985; Nixon, 1991; Hansson et al., 2004; Rempel, 2007; Nishimura et al., 2009; Ji et al., 2019; Cai et al., 2022). Depending on the complexity of the specific material parameters in the model, geometric characteristics and governing equations need to be included and solved.

Physical field models focus on the moisture, mechanical and temperature field prediction and do not predict single ice lens formation but an increasing finite volume of the soil. These are usually coupled thermo-hydro-mechanical (THM) models based on the continuum poromechanics theory. The increasing volume is described by moisture accumulation due to temperature-dependent suction (Fremond and Mikkola, 1991; Hartikainen and Mikkola, 1997; Michalowski and Zhu, 2006; Zhang and Michalowski, 2015; Sweidan et al., 2021).

* Corresponding author.
E-mail address: niggemann@gut.rwth-aachen.de (K. Niggemann).
Peer review under responsibility of Institute of Rock and Soil Mechanics, Chinese Academy of Sciences.

https://doi.org/10.1016/j.jrmge.2023.07.004
1674-7755 © 2023 Institute of Rock and Soil Mechanics, Chinese Academy of Sciences. Production and hosting by Elsevier B.V. This is an open access article under the CC BY-NC-ND license (http://creativecommons.org/licenses/by-nc-nd/4.0/).

However, numerical methods require a great deal of experimental effort and specialized tests to obtain the relevant modeling parameters. Therefore, they are only used in exceptional cases. Additionally, since the complex microscopic processes involved in ice lens formation have not yet been fully understood, parameters must be approximated or assumed for the numerical solution (Sweidan et al., 2021; Suh and Sun, 2022) and in some cases, lack physical meaning, especially when considering constitutive models. Therefore, in practice, frost heave at the surface is controlled by adapting the freezing operation using observations or using other analytical or semi-analytical solutions based on previous experience.

Han and Goodings (2006) developed a practical model for explaining frost heave in clay as a function of the freezing depth, taking into account compression settlement below the deepest ice lens but without considering explicit ice lens growth. Jiang et al. (2009), Wang et al. (2014), and Li et al. (2018) proposed analytical solutions for the freezing-temperature field of a single freezing pipe under the condition of a constant heat flow boundary. Li et al. (2018) considered the unfrozen water below freezing temperatures by a temperature-dependent soil freezing characteristic. A multi-step phase change process approximates a continuous phase change process and further transforms into a multi-phase Stefan problem in cylindrical coordinates. Cai et al. (2018, 2019) predicted the frost heaving according to the AGF freezing method that uses the stochastic medium theory for heave calculation. They not only consider the freezing process around single freezing pipes until they interconnect to a freezing wall but also the increasing thickness of the freezing wall with time. They use a flat-panel freezing theory with a heat conduction problem in a one-dimensional (1D) semi-infinite domain. For the calculation of frost heaving, their model uses the frost heave ratio ε_f as an input parameter.

Further research concerning analytical solutions of frost force focus on cold-region tunnels in the rock. Feng et al. (2019) analyzed the anisotropic frost heave of a cold-region tunnel. They derived an analytical elasto-plastic solution of the stress and deformation with Drucker-Prager criterion by modifying the constitutive equation for the frozen surrounding rock. Zhao et al. (2020) established a new model for coupled heat and moisture transfer in the freezing surrounding rock. They proposed an analytical solution in which the calculated parameters are classified into frost heave ratio, geometric parameters, and confinement strength. Lyu et al. (2020) established an analytical solution of frost heaving force and stress distribution in cold region tunnels under non-axisymmetric stress and transversely isotropic frost heave of the surrounding rock. They considered the mechanical process of freezing and expansion without constraints and inhibited frost-heaving displacement by lining and unfrozen surrounding rock. Zhu et al. (2021) studied an analytical solution to stress and deformation for noncircular tunnels in cold regions. They transformed a noncircular tunnel into a circular tunnel by conformal mapping and deduced an elastic analytic formula for a noncircular tunnel with a lining-frost heaving zone-surrounding rock system.

The explained analytical models primarily focus on frost penetration and do not explicitly consider the ice lens growth. Ji et al. (2019) introduced a numerical quasi-static model considering slowly varying segregation temperatures during ice lens formation to calculate ice lens growth. They considered a decreasing hydraulic permeability due to pore blocking and the resulting pore water pressure effect to determine the unfrozen water content in the frozen fringe. The hydraulic permeability can be considered as a function of temperature and pressure. The model offers a method to predict frost heave after reaching thermal steady-state conditions but needs several input parameters that include information about the frozen fringe.

Table 1
Analytical models for the freezing calculation from the literature.

Source	Description	Freezing calculation		
		Temperature field	Expansion/ force	Ice lens (explicit)
Konrad and Morgenstern (1980, 1981, 1982)	Development of SP theory			x
Han and Goodings (2006)	Frost heave model considering compression settlement		x	
Jiang et al. (2009)	1D freezing temperature field calculation	x		
Wang et al. (2014)	1D freezing temperature field calculation	x		
Li et al. (2018)	1D freezing temperature field calculation	x		
Cai et al. (2018, 2019)	Freezing temperature field calculation and stochastic medium theory	x	x	x (heave ratio is required)
Feng et al. (2019)	Elasto-plastic solution for frost force considering anisotropic frost heave in rock		x	
Zhao et al. (2020)	Frost force of coupled heat and moisture transfer in tunnels		x	
Lyu et al. (2020)	Frost heaving force and stress distribution under non-axisymmetric stress and transversely isotropic frost heave	x	x	
Zhang et al. (2020)	Extension of the SP in a closed system			x
Zhu et al. (2021)	Frost force and displacement for noncircular tunnels		x	
Jin et al. (2021)	SP determination by upwards-step-freezing method			x

Note: 'x' represents the selected calculation type.

The well-known approaches for ice lens calculation from the literature are the numerical rigid ice model published by O'Neill and Miller (1982, 1985) and the semi-analytical segregation potential (SP) concept from Konrad and Morgenstern (1980, 1981, 1982). These approaches are still used in practice for frost heave calculation or get improved by theoretical research.

O'Neill and Miller (1982, 1985) defined the ice lens initiation by a pressure-dependent approach. The rigid ice model explains ice lens initiation as the process where pore water pressure conditions are high enough to separate the soil particles. They introduced a neutral stress that includes ice and water pressure conditions and a semi-empirical stress partition function describing the distribution of overlying weight between pore ice and pore water in the frozen fringe. The pore water pressure is calculated by Darcy's law and the ice pressure using the Clausius-Clapeyron equation. The stress partition function is semi-empirical depending on the water content and porosity. The application of the Clausius-Clapeyron equation in the case of ice lens formation is questionable because it is only valid for equilibrium conditions. However, it is known that during freezing, transient conditions with frost penetration, increasing heaving pressure, or decreasing suction are present (Loch, 1978; Penner, 1986). Another aspect of the numerical rigid ice model is the great computational effort necessary due to the initiation and growth of individual ice lenses (O'Neill and Miller, 1985).

In the semi-analytical approach developed by Konrad and Morgenstern (1980, 1981, 1982), a soil constant, SP, is determined

with the help of frost heave tests in open system. It is a temperature-dependent approach with a segregation temperature that defines ice lens initiation. The segregation temperature is associated with the critical permeability and constant for a given soil, regardless of the temperature boundary conditions. Using this soil constant SP, the ice lens heave can be determined as a function of the present temperature gradient. Only one freezing test is necessary to obtain SP for one specific soil.

The SP approach has been used for decades to predict frost heaving in permafrost regions (Nixon, 1982; Konrad and Shen, 1996; Tiedje and Guo, 2012; Zhang et al., 2020). However, the approach was developed based on natural soil freezing and is only valid for the thermal transient state, i.e. during a moving frost line. Conversely, in AGF, not only the thermal transient state has to be taken into account. After a certain frost thickness has been reached, the frost line stays at a specific position for up to several weeks, where a thick ice lens can form. This so-called thermal quasi-steady state may lead to enormous frost heaving during construction time. For this state, the SP approach is unsuitable (Jessberger and Jagow, 1989).

Because the SP is widely accepted for engineering applications, the approach continues to be improved and extended for specific boundary conditions. For example, Jin et al. (2021) investigated the SP by an upward-step-freezing test method and Zhang et al. (2020) tested its application in closed system freezing test.

Table 1 provides a summary of the introduced analytical approaches from the literature.

Based on this shortcoming, we propose a new practical semi-analytical approach that allows the explicit prediction of ice lens heaving. It builds on the SP method and extends it to the quasi-steady state regime. Compared to numerical modeling, the advantage of a semi-analytical approach is that an experimental freezing test indirectly achieves information about unknown properties of the frozen fringe for a specific soil. This gives the approach a multifaceted application to soils known to allow ice lens formation (i.e. fine-grained materials with high saturation). The properties of the frozen fringe still need to be sufficiently and universally explored but prevailing for ice lens formation. Numerical modeling usually uses empirical relations from literature (e.g. Ji et al., 2019), which needs information about the frozen fringe difficult to explore. The validation of the semi-analytical approach presented here was carried out using 50 experiments and two different frost-susceptible soils.

The following Section 2 includes general information about the experiments used for the approach validation, the two soils used for validation, test series, and experimental conditions. Section 3 includes the general equations for the frost heave calculation that are basic for the new semi-analytical approach and hydro-mechanical aspects of ice lens formation. Further, the boundary conditions of a frozen soil column are provided. Assumptions and simplifications for the semi-analytical approach are given in Section 4. In Section 5, the semi-analytical approach for the transient and quasi-steady state is explained. Section 6 gives an overview of Konrad and Morgenstern's SP, followed by a comparison of SP and the new approach. Section 7 includes the validation of the new approach separately according to thermal conditions and for both soils. Finally, a summary and conclusions are presented in Section 8.

2. General information

The laboratory investigations focused on frost heaving with ice lens formation for different boundary conditions of AGF. The primary investigation focused on the freezing directions by freezing samples from the bottom upwards (bottom freezing, BF) and from the top downwards (top freezing, TF). For AGF conditions, the BF freezing direction, which is in the direction of the soil surface, is most critical. The water flow leading to ice lens formation was opposite to the freezing direction. During freezing, two thermal states were considered. The first one is the thermal transient state with a moving frost line. This state describes the freezing process until the frozen body's final thickness is reached. In this state, mainly pore water expansion dominates frost heaving. The amount of freezing pore water depends on several conditions, e.g. grain and pore size, solutes, freezing temperature, and overburden load. The ice lens formation is limited by the migrating frost line. In the second state, the so-called quasi-steady state, the frost line stayed at a specific position which depends on the thermal boundary conditions. This state is comparable with the holding phase at AGF, where the thickness of the frozen body is only preserved over a more extended period. Here, only ice lens formation and growth occurred. A full description of the test device, experimental test series, and soil can be found in detail in Niggemann et al. (2023). Below we introduce a summary.

2.1. Test device

Fig. 1 shows the test device used for the experiments. The cylindrical soil sample was frozen uniaxially from the top or the bottom downwards or upwards ①, while the lateral surface was insulated and fixed. The container was a cylinder consisting of 8 PVC ring elements that were able to be pulled and moved apart

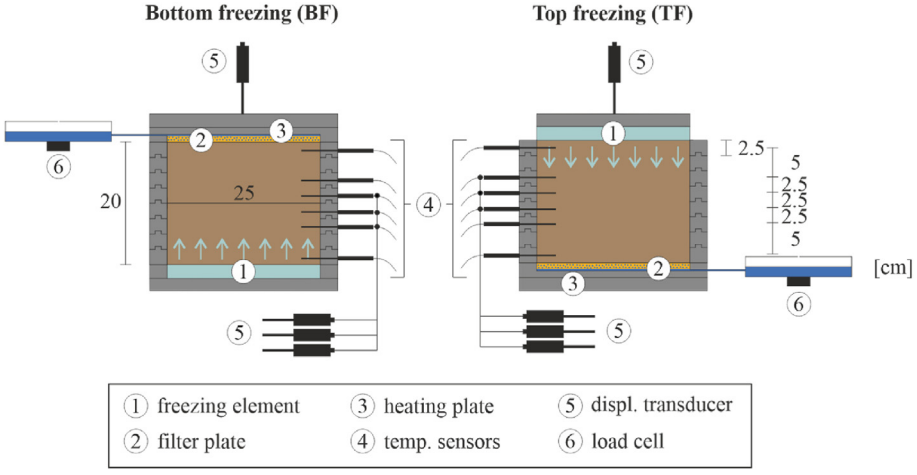

Fig. 1. Test setup for BF and TF (cf. Niggemann et al., 2023).

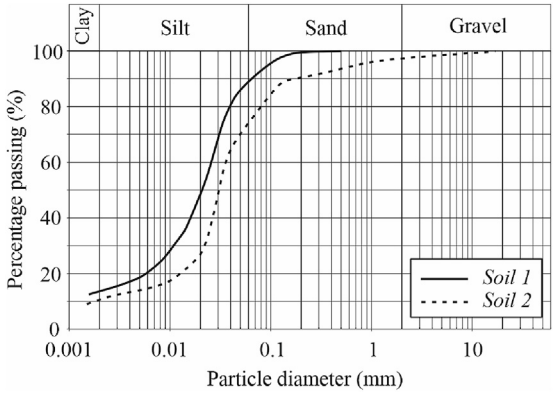

Fig. 2. Grain size distribution of soil 1 and soil 2.

Table 2
Soil parameters of soil 1 and soil 2.

Soil	$\bar{x}_{Sr}$ (%)	σ_{Sr} (%)	$\bar{x}_K$ (m^2)	σ_K (m^2)	$\bar{x}_\rho$ (g/cm^3)	σ_ρ (g/cm^3)
1	91.5	2.65	1.8×10^{-17}	7×10^{-18}	2.022	0.017
2	82.98	3.89	6×10^{-16}	5.9×10^{-16}	2.082	0.023

Table 3
Main values of the experimental parameter study for soil 1 and soil 2.

Soil	Test parameter	T_f (°C)	$T_{w,ts}$* (°C)	∇T_f (°C/cm)	n_{TF}	n_{BF}
1	T_f (°C)	−5	10.4	1	3	3
		−7.5	8.6		2	2
		−10	8		6	4
		−12.5	6.9		1	1
		−15	5.4		4	4
		−17.5	4.6		1	1
	∇T_f (°C)	−15	13.6	1.5	3	3
		−7	5.2	0.8	3	3
2	T_f (°C)	−5	9.3	1	1	1
		−10	7.3		1	1
		−15	4.7		1	1

Note: *mean values.

vertically. On the warm side was a heating plate ③ where a water reservoir provided a constant water supply (water head ≈ 1 cm) under atmospheric pressure for ice lens formation. A total load of $p = 3.6$ kPa was applied to the sample from the test apparatus elements. The tests were carried out in a climatic chamber having a constant temperature of 15 °C and humidity of 40%. The freezing process was initiated only when all sensors inside the soil reached the desired soil temperature of 15 °C which was achieved after 24 h. The soil sample was insulated before the freezing process begins to ensure only a vertical heat flow between the heating and cooling plates. Each test took up to 10 d to obtain sufficient data about ice lens formation at thermal quasi-steady state conditions.

For data recording, temperature sensors (MWT1/10, TMH GmbH, Germany) ④ were distributed over the sample height. The total uniaxial deformation and the vertical deformation of specific ring elements that were connected to the temperature sensors were measured by displacement transducers (LRW2-C-50, WayCon Positionsmesstechnik GmbH, Germany) ⑤. To determine the water inflow into the sample due to suction, the mass of the water supply was recorded by a load cell (S2, HBM, Austria) ⑥.

2.2. Test soils and conditions

2.2.1. Soil 1

Soil 1 is a lean clay (CL, unified soil classification system) primarily consisting of silt with clay and fine sand (Fig. 2). The material was prepared with a water content of 20% to ensure a high saturation and an appropriate consistency. A detailed description is in Sweidan et al. (2021) and Niggemann et al. (2023). Fig. 2 shows the grain size distribution. Table 2 contains data on soil saturation S_r, permeability K and soil density ρ of the test soil samples as mean values $\bar{x}$ with standard deviations σ. An extensive parameter study was carried out with soil 1 in Niggemann et al. (2023).

Table 3 summarises the different conditions of the 50 frost heave tests. T_f represents the freezing temperature at the top or bottom of the sample, and $T_{w,ts}$ is the warm side temperature measured by the nearest temperature sensor to the warm edge during a thermal quasi-steady state. The parameter ∇T_f is the temperature gradient along the frozen part during thermal quasi-steady state conditions. In the first tests, T_f was the varied parameter that influences the frost penetration depth. The greater the frost penetration, the shorter the unfrozen area of the soil sample or the closer the frost line to the warm edge with the water reservoir. Further tests were carried out with different temperature gradients ∇T_f along the frozen part but same frost penetration depth. Both n_{TF} and n_{BF} correspond to the number of experiments for one parameter variation.

2.2.2. Soil 2

For further validation, the semi-analytical approach was applied to a second frost-susceptible soil primary consisting of silt with sand, clay, and fine gravel constituents (Fig. 2). The water content of the soil was about 14%, and the saturation degree at approximately 83%. The test procedure was the same as soil 1.

Compared to soil 1, soil 2 is more widely graded and contains larger grains but is also characterised as CL after the unified soil classification system. Important soil parameters are listed in Table 2, and Table 3 shows the test conditions.

3. Theoretical calculation of frost heave

3.1. General equations

The calculation of total frost heave h_{tot} changes with the considered thermal state. In the transient state, frost heave comes from pore water expansion h_{PW} and ice lens formation h_{IL}. Whereas in thermal quasi-steady state conditions, only frost heave due to ice lens formation h_{IL} occurs. Hence, we have

$$h_{tot,trans} = h_{PW} + h_{IL} \tag{1}$$

$$h_{tot,stst} = h_{IL} \tag{2}$$

The heave due to pore water expansion h_{PW} is calculated for uniaxial frost heave, assuming full water saturation and a porosity φ. Since the expansion factor α during phase change from water to ice is about 9% (Hartge, 1978), we can use the frost penetration depth x to calculate the heave due to pore water expansion as

$$h_{PW} = \alpha\varphi x \tag{3}$$

The ice lens heave $h_{IL}(t)$ results from the time-dependent water flow $v_f(t)$ to the ice lens multiplied by the expansion factor α at the phase change from water to ice:

$$h_{IL}(t) = \int_0^t v_f(t)\mathrm{d}t(1+\alpha) \tag{4}$$

The Darcy's law determines the flow velocity of the free water $v_f(t)$ used for ice lens formation with Δh as the potential difference expressed as a water head and Δl as flow length:

$$v_f = k\frac{\Delta h}{\Delta l} \tag{5}$$

The hydraulic conductivity k includes all influences that the soil causes on the movement of water and can also be written as intrinsic permeability K taking into account the fluid density ρ, the dynamic fluid viscosity η, and the acceleration due to gravity g (Hartge 1978):

$$K = k\frac{\eta}{\rho g} \tag{6}$$

Considering 1D vertical water flow through different soil layers, the frozen fringe is assumed to be a soil layer with low permeability. Due to a hydraulic head, the vertical flow velocity is the same through different layers (series model). We assume this is true during the thermal steady state where the temperatures are constant throughout, but also during thermal transient state. This is because we observe a very small water accumulation during thermal transient freezing (less than 5%), as shown in Sweidan et al. (2021). However, the pressure reduction and the permeabilities through the different soil layers are not constant. The pressure reduction occurs primarily in very impermeable soils (von Soos and Engel, 2017). In a semi-frozen soil column as that considered here (see Fig. 3), the water flows from the unfrozen soil (uf) through the frozen fringe (ff) towards the ice lens (IL) or frozen soil (f) at a constant Darcy velocity v_f, at any given time, can be calculated by

$$v_f = k_{ff}\frac{\Delta h_{ff}}{l_{ff}} = k_{uf}\frac{\Delta h_{uf}}{l_{uf}} \tag{7}$$

3.2. Hydro-mechanical aspects of ice lens formation

Fig. 3 shows the characteristics of soil freezing from the bottom upwards as it occurs during AGF. It is essential to mention that the dimensions are inaccurate scale. In reality, the frozen fringe and the ice lens are very small compared to the frozen and unfrozen areas. In this simplified case, infinite water availability at the ground surface is assumed, and the water migrates due to a suction gradient towards the ice lens. This occurs regularly in natural conditions.

Konrad and Morgenstern (1980) defined the unfrozen soil and frozen fringe as the active part because the relevant mechanism of water migration towards the ice lens formation occurs within these areas. In the passive frozen part, it is assumed that no water migration takes place. Fig. 3 overview temperatures T, permeabilities K, hydraulic heads h and their resulting gradients ∇h, and flow velocities v_f along the frozen fringe l_{ff}, the unfrozen soil part l_{uf}, the ice lens l_{IL} and the frozen soil part l_f.

The temperature gradient ∇T along the frozen fringe is assumed to be the same along the unfrozen area by Konrad and Morgenstern (1980) because the boundary temperatures of the frozen fringe (0 °C and the ice lens temperature) are very close, which justifies a thermal conductivity similar to the unfrozen zone. Furthermore, the temperature gradients along the active and passive parts can each be assumed to be linear, which is confirmed by the temperature measurements along the length of the test soil samples (exemplary for one test in Fig. 4). Linear gradients are also assumed by Konrad and Morgenstern (1980).

The hydraulic head h (includes cryogenic suction) at the ice lens depends mainly on the adsorption forces which bound the water molecules to the soil particles. The ice lens grows by attracting these strong bounded water molecules at the bottom of the ice lens. The water film thickness around the particles is maintained by drawing in free water from the unfrozen region. The thinner the water film around the particles due to decreasing temperature conditions, the greater the adsorbed forces or suction. Thus, maximum suction occurs on the warm side of the ice lens (Kaplar, 1970; Sheng et al., 1995; Wilen and Dash, 1995; Rempel, 2010). The suction decreases rapidly until the frost line (0 °C-isotherm) is reached. In very frost-susceptible soils, atmospheric pressure is not reached at the frost line, and a suction gradient over the unfrozen part is degraded along the entire fine layer (Konrad, 1989; Arenson et al., 2008; Zhang et al., 2020). In Fig. 3, the water head at the ground surface is zero.

The hydraulic gradient ∇h depends on water head conditions and the length l of each zone and indicates the water flow velocity v_f when multiplied by the permeability K.

4. Assumptions and simplifications

Considering continuity with mass conservation, the water flow through the boundaries between the ice lens/frozen fringe, frozen fringe/unfrozen soil, and unfrozen soil/water reservoir is the same and, thus, allows calculating the ice lens heave from the flow conditions in the unfrozen soil:

$$v_{f,uf} = K_{uf}\frac{\rho g}{\eta}\frac{\Delta h_{uf}}{l_{uf}} = K_{uf}\frac{\rho g}{\eta}\frac{h_0 - h_{ref}}{l_{uf}} \tag{8}$$

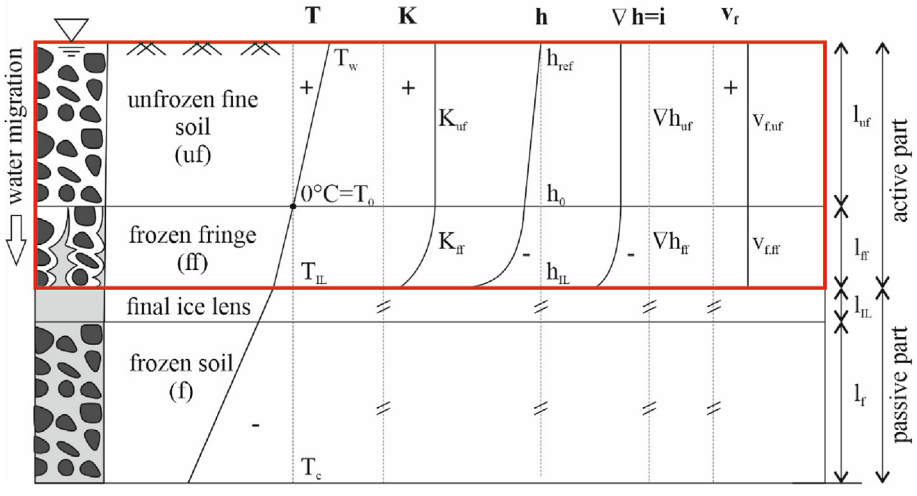

Fig. 3. Characteristic of a bottom upwards frozen soil column.

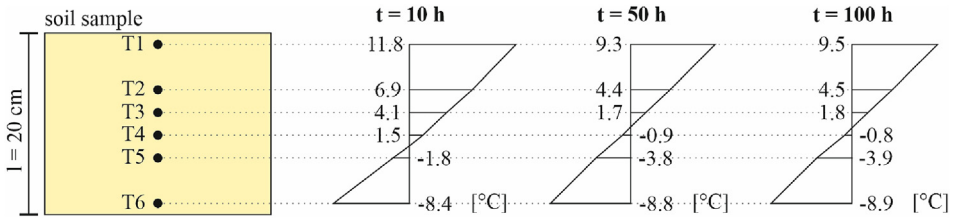

Fig. 4. Temperature measurements along the sample length l for different freezing time steps with a cooling temperature of −10 °C. The permeability K at the warm side of the ice lens is very low but increases towards the unfrozen area until it stays constant along the unfrozen area.

The hydraulic head at the reference height h_{ref}, which is the level of the ground surface in the case of Fig. 3, is equal to the atmospheric pressure. These conditions correspond to the experimental conditions. The hydraulic head at the 0 °C-isotherm h_0 is unknown but assumed to be the same for one specific soil because the suction magnitude is connected to the water film thickness, which is temperature-dependent but also related to the mineralogy of the soil grains and their size and morphology (Hartge, 1978). The generalized Clausius-Clapeyron equation is widely used to describe phase change processes between ice and water in soils (Edlefsen and Anderson, 1943; Biermans et al., 1978; Loch, 1978; O'Neill and Miller, 1985; Penner, 1986; Black, 1995; Ma et al., 2015). However, in the generalized Clausius-Clapeyron equation, the atmospheric pressure is achieved at 0 °C, meaning no suction would occur in the unfrozen region. The application is, therefore, not suitable for these boundary conditions.

After assuming a linear temperature profile along the unfrozen part, the length of the unfrozen soil l_{uf} can be calculated by the temperature difference ΔT_{uf} between the frost line ($T_0 \approx 0$ °C) and warm side boundary (T_w) and the temperature gradient ∇T_{uf} along the unfrozen soil:

$$l_{uf} = \frac{\Delta T_{uf}}{\nabla T_{uf}} = \frac{T_w - T_0}{\nabla T_{uf}} \tag{9}$$

4.1. Thermal transient state

For thermal transient conditions, the length of the unfrozen soil l_{uf} changes with time due to frost penetration. Thus, the temperature gradient ∇T_{uf} is also time-dependent. Depending on the set boundary conditions, the temperature difference ΔT_{uf} may also be time-dependent in this state. Considering AGF with low freezing temperatures and fast freezing velocities, only very thin ice lenses are formed. It is therefore assumed that the consolidation effect during the formation of these thin ice lenses is negligible. Using Eqs. (4) and (9), the ice lens heave during thermal transient state can be calculated as follows:

$$h_{IL}(t) = \int_0^t k_{uf} \frac{\Delta h_{uf}}{\Delta T_{uf}(t)} \nabla T_{uf}(t)(1+\alpha)\mathrm{d}t \tag{10}$$

4.2. Thermal quasi-steady state

For quasi-steady state conditions, constant temperature boundary conditions are assumed, i.e. the length l_{uf} and the temperature gradient ∇T_{uf} of the unfrozen part do not change.

During thermal quasi-steady state, one last ice lens grows over a specific period. Thus, local consolidation can no longer be neglected, e.g. Xia et al. (2005) and Zhang et al. (2016). This affects the hydraulic conductivity in the frozen fringe with time. For AGF near the surface in fine-grained soil, air inclusions are still present below the groundwater surface (Hartge, 1978). During water flow towards the ice lens, soil air may be transported by the sucked water and accumulates at the impermeable ice lens (Fig. 5). Arenson and Sego (2006) investigated an increasing amount of trapped air at the ice lens by taking high-resolution images during freezing at high but not completely saturated soil. This entrapped soil air accumulates at the warm end of the ice lens and forms a barrier reducing the flow velocity. They are observed as white threads appearing in the ice lens parallel to the direction of growth (Fig. 6). The air accumulation in the frozen fringe reduces the hydraulic conductivity of the soil with time.

To cater for this, the frozen fringe can be compared to a clogging filter with a decreasing hydraulic conductivity, whereby the hydraulic height changes in a time-dependent way as a result of the potential reduction. This also affects the hydraulic head between the frozen fringe and unfrozen part and, thus, the hydraulic gradient in the unfrozen soil. This time-related ice lens heave is given in Eq. (11). The difference in the thermal transient conditions in Eq. (10) is given by the time-dependent hydraulic head instead of time-dependent temperature conditions.

$$h_{IL}(t) = \int_0^t k_{uf} \frac{\Delta h_{uf}(t)}{\Delta T_{uf}} \nabla T_{uf}(1+\alpha)\mathrm{d}t \tag{11}$$

Further, we cater that the frost heave and time-dependent water flow during geometrical change by clogging are not proportional to the hydraulic gradient. Kutílek (1972) reported variations from a proportional relationship between water flow and hydraulic gradient due to clogging pores in fine soil material such as clay or bentonite, similar to the soil in this paper. Fig. 7 also shows the under-proportional relationship for soil with a high clay content (≈30%) in tests conducted by Miller and Low (1963). As the hydraulic gradient increases, channels between large pores become unblocked, resulting in disproportionate water flow with increasing hydraulic gradient. Due to the ice lens barrier, disproportionate water flow cannot occur near the ice lens.

We cater to this by including an exponent n in Eq. (12) as proposed, e.g. by Kutílek (1972) or Busch et al. (1993). The parameter n describes the nonlinear relation between the flow rate and the hydraulic gradient. It generally considers inertial forces ($n < 1$, flow grows less than proportional to the hydraulic gradient) and adhesive forces ($n > 1$, flow grows more than proportional to the hydraulic gradient). Since the frost-susceptible soil usually has a greater content of fines that may cause geometrical changes like clogging, the exponent should be smaller than one ($n < 1$). Since the ice lens formation process during the thermal transient state is interrupted by the moving frost line, the effect of geometrical changes expressed by the parameter n can be neglected. This especially applies to AGF with great freezing velocities.

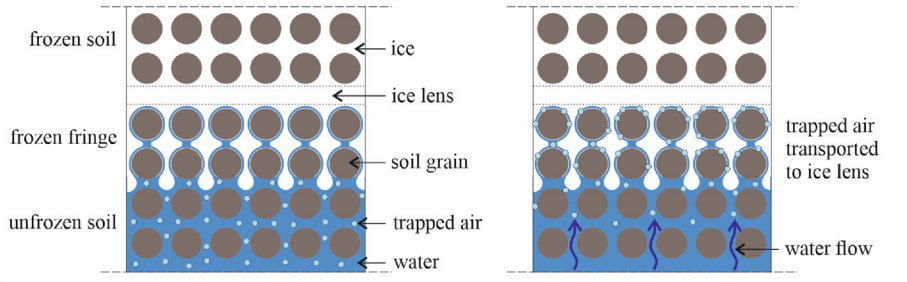

Fig. 5. Accumulation of trapped air at the bottom of the ice lens due to water transport.

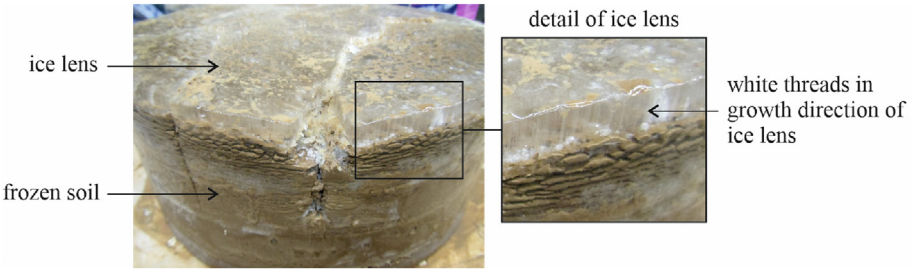

Fig. 6. White threads due to entrapped air during ice lens formation.

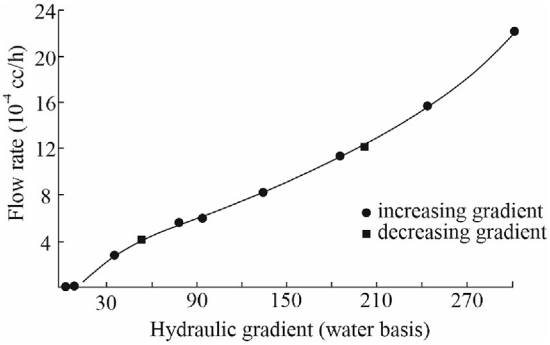

Fig. 7. Flow rate-gradient relationship for a clay paste (after Miller and Low, 1963).

$$h_{IL}(t) = \int_0^t k_{uf}\left(\frac{\Delta h_{uf}(t)}{\Delta T_{uf}}\nabla T_{uf}\right)^n (1+\alpha)\mathrm{d}t \tag{12}$$

5. Semi-analytical approach

5.1. Thermal transient state

Based on Eq. (10), the hypothesis is that the resulting value of Eq. (13) is constant, C, for one soil under different thermal boundary conditions. Because the hydraulic conductivity k_{uf} and the difference of the hydraulic head in the unfrozen area Δh_{uf} do not change due to different thermal boundary conditions (cf. section 4). It uses the ice lens heave $h_{IL}(t)$ and the time-dependent thermal boundaries ($\Delta T_{uf}(t)$ and $\nabla T_{uf}(t)$), common values to measure during one frost heave test. Conversely, values of the hydraulic conductivity k_{uf}, the expansion factor α, and the difference in the hydraulic head for the unfrozen zone Δh_{uf} are challenging to measure directly from tests. Especially the measurement of the hydraulic head at the moving 0°C-isotherm is critical and not standard.

$$\frac{\mathrm{d}h_{IL}(t)}{\mathrm{d}t}\frac{\Delta T_{uf}(t)}{\nabla T_{uf}(t)} = k_{uf}\Delta h_{uf}(1+\alpha) = C \tag{13}$$

Fig. 8 shows the left term of Eq. (13) plotted against time for the tests at different bottom freezing temperatures. Qualitatively, the results for TF are very similar and can be found in Appendix A (Fig. A.1). The ice lens heave is calculated by the difference of measured total heave and pore water expansion (cf. Eq. (1)) which is calculated using Eq. (3). A measurement of pure ice lens heave during thermal transient conditions was not applicable during the tests. Thus, the accuracy of calculated ice lens heave for the thermal transient state may be affected. For calculating the temperature gradient in the unfrozen soil part, the temperature at the frost line is assumed to be 0 °C, and temperature sensors measure the warm side of the sample during the experiments. The time-dependent temperature analysis of the sample allows the determination of the unfrozen soil length (detailed explanations can be found in Niggemann et al. (2023)). At the beginning of freezing, only pore

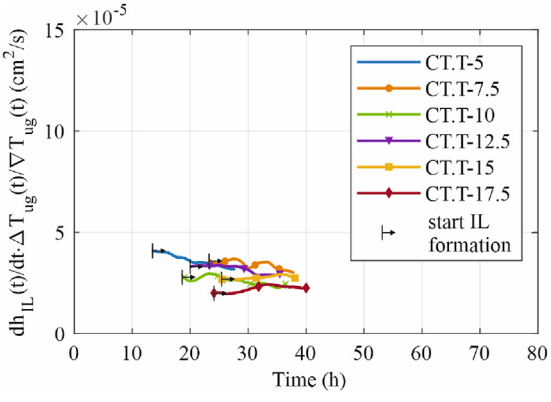

Fig. 8. C-values over time for the thermal transient state and BF (soil 1).

water expansion occurs (flat line for the initial part of each curve in Fig. 8). As time passes, the ice lens initiation occurs with an increasing heave difference until a maximum value is reached. At the end of transient freezing, the curves achieve similar values despite different boundary freezing temperatures. The mean value of the approximately constant parts given in Fig. 8 (right) is 3.04×10^{-5} cm^2/s, and the standard deviation (SD) 5.14×10^{-6} cm^2/s (for the calculation, the constant parts are considered over a same period). The similar curve progression confirms the hypothesis of a constant, C, independently from thermal boundary conditions for the end of transient freezing given in Eq. (13).

Fig. 9 shows the linear relationship between the ice lens heave derivation $\mathrm{d}h_{\mathrm{IL}}/\mathrm{d}t$ and the reciprocal of the flow path $1/\ l_{\mathrm{uf}}$ for the end of transient freezing for the experimental BF-tests with different thermal boundary conditions given in Table 3. At the end of transient freezing, it can be assumed that heave only comes from ice lens formation. Before, there was still volume expansion due to frost penetration. The linear regression in Fig. 9 correctly captures the fitted linear relationship, validated by the very small SSE (sum of squares error). It indicates that the values do not vary widely around the fitted line. The R^2 value of 0.49 is primarily due to the dispersion of the values at points, which are independent of the magnitude. Therefore, the linear trend as an average value is assumed to be appropriate for the used data.

For the calculation of C, only the temperature at the warm side of the sample, the temperature gradient along the unfrozen length, and the ice lens heave must be measured during one frost heave test. The total heave measurement can replace the determination of ice lens heave because the constant C is calculated for the end of transient freezing where the total heave is equivalent to the ice lens heave.

There is only one test required to determine C. If C is known for one soil, the ice lens heave can be calculated for different thermal boundary conditions without further soil freezing tests using the following expression:

$$h_{\mathrm{IL}}(t) = C \int_0^t \frac{\nabla T_{\mathrm{uf}}(t)}{\Delta T_{\mathrm{uf}}(t)} \mathrm{d}t \tag{14}$$

5.2. Thermal quasi-steady state

Rearranging Eq. (12) according to the known (measurable during frost heave test) and unknown parameters, the power function in Eq. (15) can be found. In contrast to the thermal transient state, the temperature conditions (ΔT_{uf} and ∇T_{uf}) are constant. The ice lens heave h_{IL} equals the total heave since there is no frost

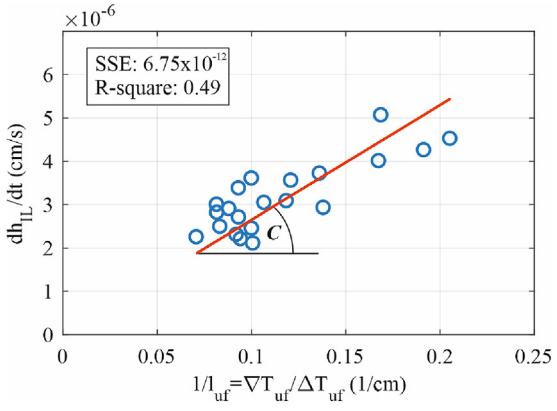

Fig. 9. Linear last-square regression at the end of thermal transient state for BF (soil 1) with $C = 2.65 \times 10^{-5}$ cm^2/s.

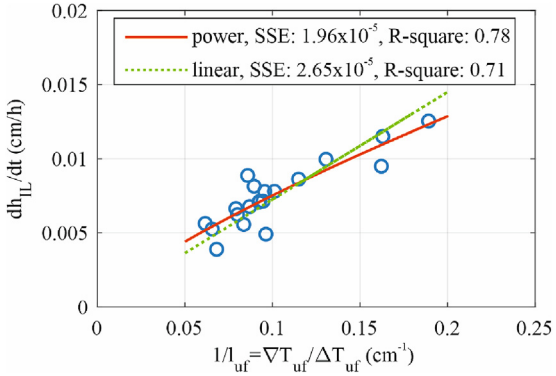

Fig. 10. Non-proportional relation between the time derivation of the ice lens heave plotted against the reciprocal of the flow path for t = 150 h during thermal quasi-steady state for BF (soil 1) (n = 0.7744).

penetration, thus no pore water expansion occurs. The hydraulic head at the 0 °C-isotherm changes with time due to potential reduction in the frozen fringe (see Section 4.2 for explanation). The hypothesis is formulated that the resulting value of Eq. (15) is a time-dependent function $f(t)$ and valid for one specific soil for different temperature conditions.

$$\frac{\mathrm{d}h_{\mathrm{IL}}\ (t)}{\mathrm{d}t}\left(\frac{\Delta T_{\mathrm{uf}}}{\nabla T_{\mathrm{uf}}}\right)^n = k_{\mathrm{uf}} \Delta h_{\mathrm{uf}}(t)^n (1+\alpha) = f(t) \tag{15}$$

To verify the hypothesis, the exponent n must first be determined, which considers the nonlinear relationship between the hydraulic conductivity and the hydraulic gradient. The nonlinearity can be transferred to the heave rate and the reciprocal of the flow path of water feeding the ice lens. In Fig. 10, the time derivation of the ice lens heave $\mathrm{d}h_{\mathrm{IL}}/\mathrm{d}t$ is plotted against the reciprocal of the flow path $1/l_{\mathrm{uf}}$ or $\nabla T_{\mathrm{uf}}/\Delta T_{\mathrm{uf}}$, respectively. The nonlinear course of the experimental results for different thermal conditions confirms the assumption of a power function due to the non-proportional relation between water flow velocity and hydraulic gradient. A very similar result was investigated for TF, given in Appendix A (Fig. A2). A linear progression through the origin (if the unfrozen length l_{uf} is large, the ice lens heave gradient $\mathrm{d}h_{\mathrm{IL}}/\mathrm{d}t$ runs towards zero) would also fit for smaller values of $1/l_{\mathrm{uf}}$. However, it would overestimate the values as $1/l_{\mathrm{uf}}$ increases.

Fig. 10 shows the conditions at the end of the freezing test 150 h after the beginning of thermal quasi-steady state. However, all executed experiments showed that the power function in Fig. 10, which represents the nonlinear relationship between flow velocity (= heave rate) and the hydraulic gradient (cf. Section 4.2), slightly changes with time during a thermal steady state. This can be empirically considered by the coefficients $m(t)$ and $n(t)$ in Eq. (16) calculated for different time steps from the beginning of the thermal steady state (note that $f(t)$ is valid for one specific soil for different thermal conditions). For the calculation, at least two frost heave tests with information on h_{IL}, ∇T_{uf}, and ΔT_{uf} are required for each time step.

$$\frac{\mathrm{d}h_{\mathrm{IL}}(t)}{\mathrm{d}t} = m(t)\left(\frac{\nabla T_{\mathrm{uf}}}{\Delta T_{\mathrm{uf}}}\right)^{n(t)} f(t) \tag{16}$$

In Figs. 11 and 12, $m(t)$ and $n(t)$ were calculated for different time steps (t = 25, 50, 75, 100, 125 and 150 h) to consider the time-dependent progression between the heave rate and the reciprocal of the unfrozen soil length. Since both are power functions, Eqs.

(17) and (18) can be written, which includes four parameters to be fitted (a, b, c and d).

$$m(t) = at^b \tag{17}$$

$$n(t) = ct^d \tag{18}$$

The absolute values of $m(t)$ and $n(t)$ for the specific time steps in Figs. 11 and 12 just slightly change with time (coefficient of variation $CV_m = 26.2\%$ and $CV_n = 6.9\%$). Therefore, it is valid to simplify the correlation by using the mean values $\overline{m}$ and $\overline{n}$ instead of the functions $m(t)$ and $n(t)$ in Eq. (16). For verification, Fig. A.3 in Appendix A exemplary provides the results of the mean average error (MAE) between calculated and measured frost heave data for different freezing temperatures (the data refer to BF of soil 1 in Fig. 19). First, the frost heave calculation was done by using the functions $m(t)$ and $n(t)$ and, second, it was carried out by using the mean values $\overline{m}$ and $\overline{n}$. The low deviation between the MAEs confirm the validity to use the mean values $\overline{m}$ and $\overline{n}$ in Eq. (16). For the verification of the approach in Section 7, the functions $m(t)$ and $n(t)$ were used.

Fig. 13 shows $f(t)$ for different bottom freezing temperatures considering the time dependency of the power functions. The right side of Fig. 13 shows a zoomed section with the mean curve (mean) and the standard deviation (SD) with an average value of 1.02×10^{-1} cm^2/h. Independent of the temperature boundary conditions, $f(t)$ collapses into a single relationship confirming the assumption. A similar evaluation for TF tests is given in Appendix A (Fig. A.4).

For the application of the semi-analytical approach, it is necessary to calculate a power function analogous to Fig. 10 from at least two experimental trials with different temperature boundary conditions. These two trials also allow the calculation of $\overline{m}$ and $\overline{n}$ for the period of the experimental tests.

Subsequently, the function $f(t)$ is determined with one of the experimentally conducted tests designated as a reference experiment:

$$\int_0^t f(t)\mathrm{d}t = h_{\mathrm{IL}}(t)\frac{1}{\overline{m}}\left(\frac{\Delta T_{\mathrm{uf}}}{\nabla T_{\mathrm{uf}}}\right)^{\overline{n}} \tag{19}$$

The frost heave prediction for different thermal boundary conditions can be solved analytically. For this purpose, only the temperature on the warm side and the temperature gradient in the unfrozen soil must be provided, which are constants in the thermal quasi-steady state:

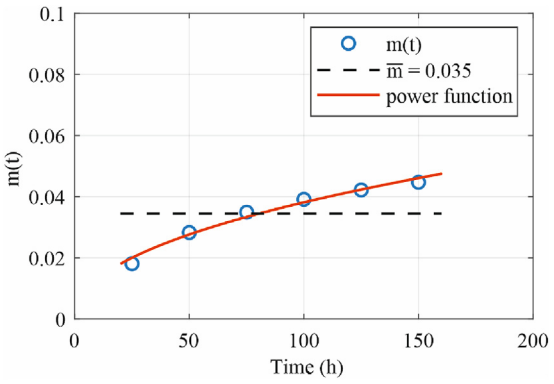

Fig. 11. Time-dependent coefficient $m(t)$ as power function with $a = 0.0045$ and $b = 0.4654$ for BF and soil 1 ($SSE = 9.34 \times 10^{-6}$, $R^2 = 0.98$).

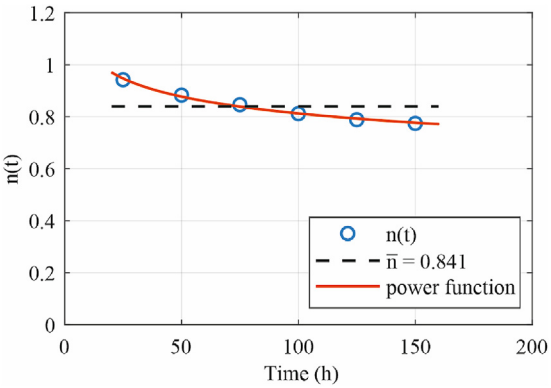

Fig. 12. Time-dependent exponent $n(t)$ as power function with $c = 1.3535$ and $d = -0.1107$ for BF and soil 1 ($SSE = 1.41 \times 10^{-4}$, $R^2 = 0.99$).

$$h_{\mathrm{IL}}(t) = \overline{m}\left(\frac{\Delta T_{\mathrm{uf}}}{\nabla T_{\mathrm{uf}}}\right)^{\overline{n}} \int_0^t f(t)\mathrm{d}t \tag{20}$$

5.3. Application of the semi-analytical approach

For the total frost heave calculation of an AGF, the thermal transient and the thermal steady state needs to be considered. The definitions of both states are given in Section 2.

Fig. 14 provides a flow chart for applying the new semi-analytical approach. Two frost heave tests with the same freezing direction in an open system and an external water source to feed ice lenses are necessary. The freezing direction depends on the in situ conditions, but for AGF, bottom freezing (BF) is recommended. The thermal boundary conditions of both tests must vary to reach different frost penetration depths. As a result of each test, the total heave $h_{\mathrm{tot}}(t)$, the temperature difference between the frost line and warm side boundary ΔT_{uf}, and the temperature gradient along the unfrozen soil ∇T_{uf} need to be measured.

For calculating the thermal transient coefficient C, only the results of one frost heave test are needed. The transient freezing period is defined by t_{ts}. The transition from thermal transient to thermal steady state occurs when the temperature gradient in the unfrozen area no longer changes. Due to this criterion, both states can be considered separately.

At the thermal steady state, the total heave $h_{\mathrm{tot}}(t_{\mathrm{ss}})$ equals the ice lens heave $h_{\mathrm{IL}}(t_{\mathrm{ss}})$. Because only one ice lens is formed over a period, time-dependent changes in the nonlinear relationship between flow velocity (= heave rate) and the hydraulic gradient are additionally considered by the mean values $\overline{m}$ and $\overline{n}$. For the calculation of the mean values, the coefficients m_i and n_i must be solved for different time steps t from the beginning of the thermal steady state by creating power functions for each time step in accordance to Fig. 10. Therefore, for the calculation of m_i and n_i, the second frost heave test is needed. With the created mean values of m_i and n_i, the function $f(t_{\mathrm{ss}})$ can be calculated.

The coefficient C, the function $f(t_{\mathrm{ss}})$, and the coefficients $\overline{m}$ and $\overline{n}$ are valid for one specific soil under a defined freezing direction. Using these, the ice lens heave for different thermal boundary conditions can be calculated. In the thermal transient state, the pore water expansion needs to be considered to calculate the total heave $h_{\mathrm{tot}}(t_{\mathrm{ts}})$.

Finally, the total frost heave $h_{\mathrm{tot}}(t)$ is calculated by the heaving components $h_{\mathrm{tot}}(t_{\mathrm{ts}})$ and $h_{\mathrm{tot}}(t_{\mathrm{ss}})$.

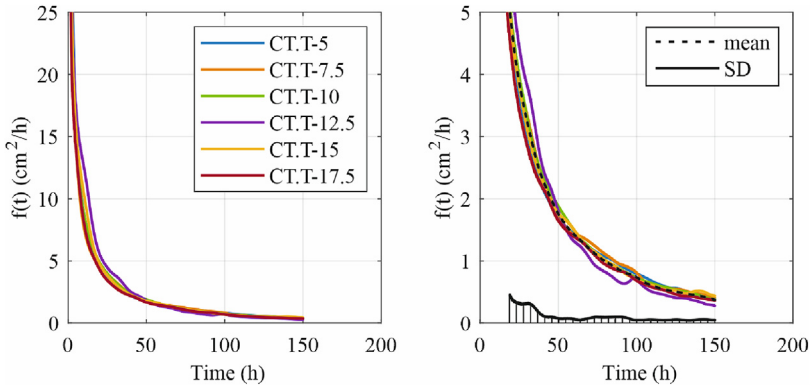

Fig. 13. $f(t)$ values over time for the thermal quasi-steady state and BF (soil 1).

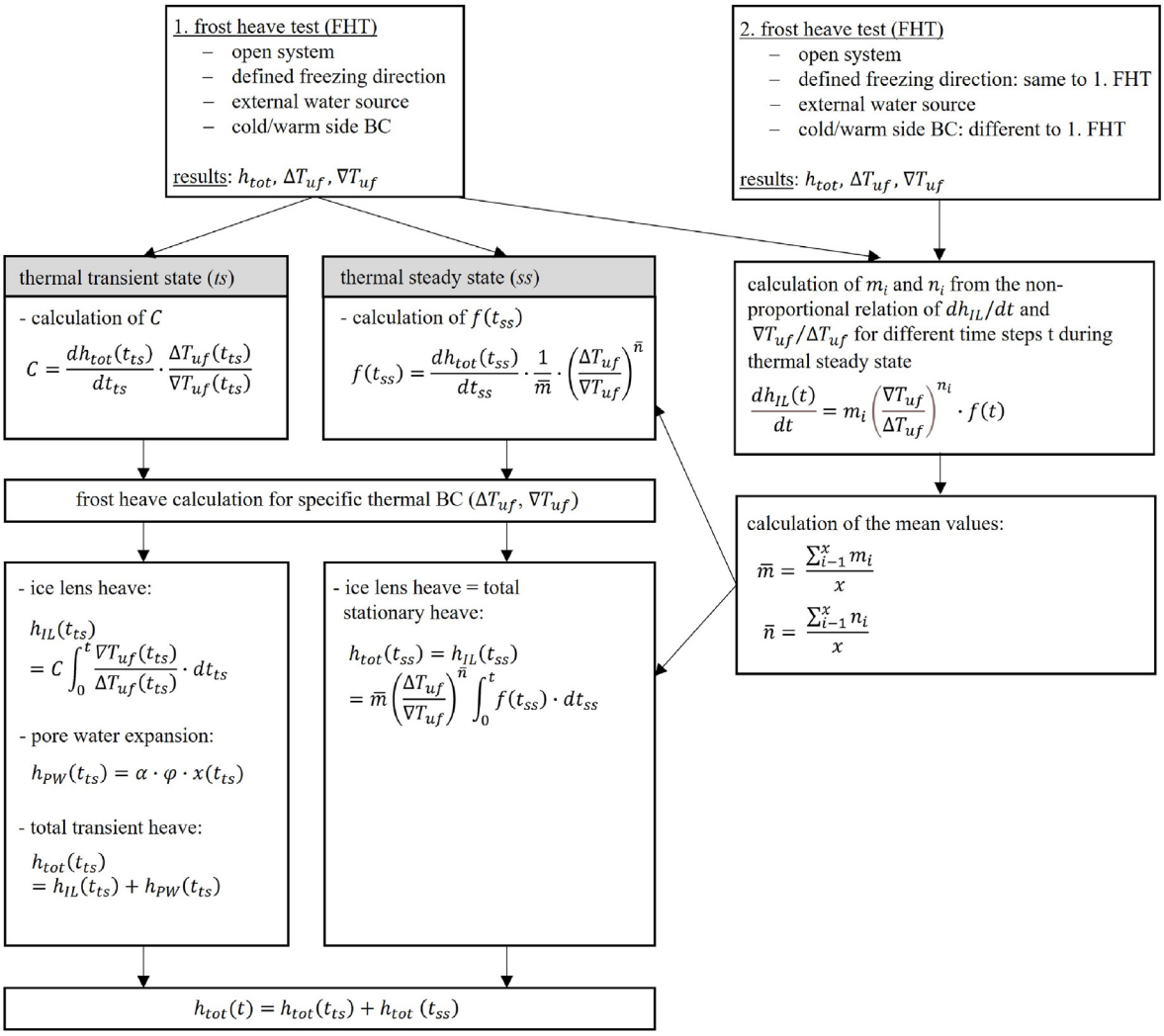

Fig. 14. Flow chart for frost heave calculation using the semi-analytical approach.

6. New semi-analytical approach vs. SP for thermal transient freezing

The SP after Konrad and Morgenstern (1980, 1981, 1982) is a practical approach to determining ice lens formation in the thermal transient state. They separate the soil into an inactive layer, the frozen part, and an active layer, consisting of the frozen fringe and the unfrozen part. The active part is characterized by a continuous water flow and accumulation only at the ice lens. The SP includes the unknown properties of the frozen fringe. The water that enters the frozen fringe per time unit corresponds to the 1D frost heave (Eq. (4)).

Conversely to the semi-analytical approach presented in this paper, Konrad and Morgenstern (1980, 1981, 1982) focused on the characteristics of the frozen fringe instead of the unfrozen soil part for calculating the water flow velocity $v_f(t)$. They assumed a mean constant permeability along the frozen fringe and a linear suction profile with atmospheric pressure on the warm side of the frozen fringe. Then, using Darcy's law, the water flow velocity $v_f(t)$ becomes

$$v_f(t) = \frac{\Delta h_{ff}}{|T_{IL}| / \nabla T_{ff}(t)} \overline{k_{ff}} \tag{21}$$

with

$$\frac{|T_{IL}|}{\nabla T_{ff}(t)} = l_{ff}(t) \tag{22}$$

where Δh_{ff} is the potential difference in the frozen fringe, T_{IL} is the ice lens temperature, and $\overline{k_{ff}}$ is the mean hydraulic conductivity along the frozen fringe. These parameters are assumed to be constant for one soil and result in the soil constant *SP*, which is calculated for the end of transient freezing (Konrad and Morgenstern, 1980) (Fig. 15).

The frost heave due to ice lens formation for one specific soil depends on the temperature gradient in the frozen fringe ∇T_{ff}, which is assumed to be similar to the temperature gradient in the unfrozen part ∇T_{uf}. Therefore, for the end of transient freezing, $t_{tf,end}$ applies

$$v_0\left(t_{tf,end}\right) = SP \nabla T_{uf}\left(t_{tf,end}\right) \tag{23}$$

The constant SP is defined for the end of transient freezing, where the assumptions made by Konrad and Morgenstern (1980) for the conventional SP are valid. During the thermal transient state, the SP varies with time, but at $t_{tf,end}$, the SP is an intrinsic physical value and independent of boundary temperature conditions (Konrad and Morgenstern, 1980; Zhang et al., 2020; Jin et al., 2021). Defining the time near the thermal steady state yields a representative SP for engineering design and frost heave prediction in the field. Jin et al. (2021) defined the time by temperature observations and determinations when the last ice lens begins to form.

The main difference to the semi-analytical approach is the focus on the frozen fringe without consideration of the unfrozen part. This applies when zero suction can be assumed at the frost line. The variable that controls the frost heave is thus the temperature gradient.

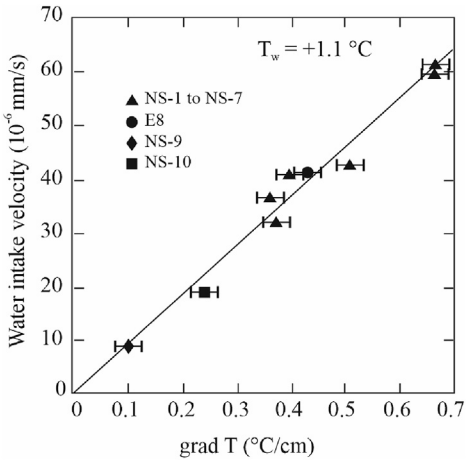

Fig. 15. Linear relationship between water intake velocity and the temperature gradient for the end of transient freezing (Konrad and Morgenstern, 1980).

Konrad and Morgenstern (1980) assumed that the temperature gradient in the frozen fringe is approximately the same as that in the unfrozen region near thermal steady state conditions. However, the executed experiments in Table 3 have shown that different ice lens thicknesses were reached with the same temperature gradient but different absolute freezing and heating temperatures or flow path lengths, respectively. Furthermore, studies on fine material have discussed suction in the unfrozen part in open systems (Sheng et al., 1995; Han and Goodings, 2006; Arenson et al., 2008; Zhang et al., 2020). For example, Han and Goodings (2006) showed that a low permeability caused the clay to behave as a closed system concerning water flow, even in an open system test. Sheng et al. (1995), Arenson et al. (2008), and Zhang et al. (2020) showed the suction at the interface between the frozen fringe and the unfrozen soil. However, the suction is reduced until the sample edge is reached. Therefore, the assumption of zero suction at the frost line does not hold for this type of material as long as a thick layer of unfrozen soil is still present. In summary, Konrad and Morgenstern's approach is limited when the suction at the frost line occurs. In this case, the flow path length of the freezing water must be considered.

Fig. 16 compares the ice lens heave derivation dh_{IL}/dt using the SP approach (left) and the new semi-analytical approach (right, corresponds to Fig. 9) explained in Section 5.1 for the end of transient freezing. Following Jin et al. (2021), time is defined by temperature measurements. When the penetration velocity of the frost line approaches zero, the transition from the thermal transient to the thermal steady state occurs (cf. Sweidan et al., 2021). For the SP determination, the temperature gradient along the unfrozen part ∇T_{uf} is considered on the abscissa. Compared to the new semi-analytical approach (Fig. 16, right), which additionally takes into account the temperature difference along the unfrozen soil, the proportional correlation of the SP (Fig. 16, left) shows less agreement with the test results under the specific boundary conditions given here. The negative R^2 value of the ascending SP fitting curve is due to a poor approximation. The TF calculation yields a similar result and can be found in Appendix A (Fig. A. 5).

7. Verification of the semi-analytical approach

In the following, primary BF tests are used for verification since this freezing direction is most critical for AGF. The TF results are qualitatively similar to the presented BF results and listed in Appendix A.

7.1. Thermal transient state

The calculation of frost heaving needs one experimental frost heave test to determine the constant *C* (Eq. (13)). *C* is calculated for the end of transient freezing by the frost heave h_{IL}, e.g. measured by a displacement transducer, and the reciprocal of the unfrozen soil length l_{uf}, e.g. determined by temperature measurements. Instead of $1/l_{uf}$, the thermal quotient $\nabla T_{uf}/\Delta T_{uf}$ can be determined by the temperature gradient in the unfrozen part and the warm side temperature boundary condition (assuming 0 °C at the frost line). Having *C*, one can calculate frost heaving due to ice lens formation under different thermal boundary conditions (Eq. (14)). The frost heave due to pore water expansion must be considered in the thermal transient state by Eq. (3). The presented soils have a mean saturation of 91.5% (soil 1) and 83% (soil 2) (Table 2). These unsaturated conditions impact the heave calculation of the pore water expansion due to consolidation effects and ice expansion into air-filled pores. These effects are not considered in the applied Eq. (3) because this paper focuses on ice lens heaving. Using Eq. (3), the calculated pore water expansion overestimates the measured data but provides conservative results.

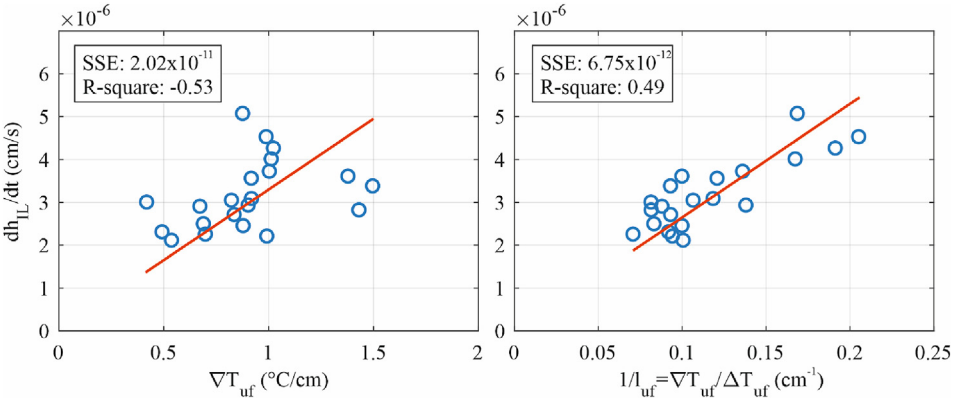

Fig. 16. SP (left) vs. new analytical approach (right) for BF conditions (soil 1) at the end of transient freezing ($SP = 3.3 \times 10^{-6}$ cm^2/(s °C), $C = 2.65 \times 10^{-5}$ cm^2/s).

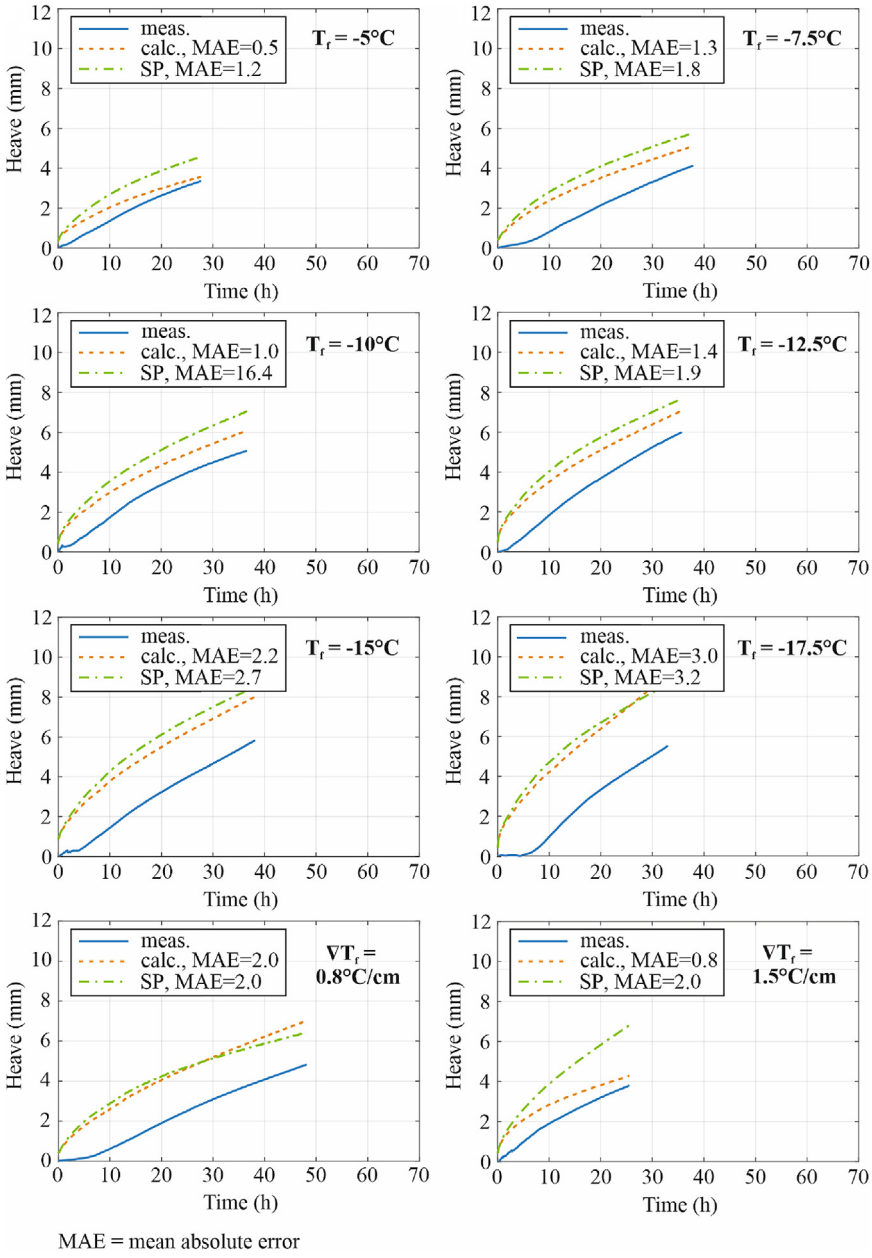

Fig. 17. Validation of semi-analytical approach for the thermal transient state under different temperature conditions for BF (soil 1).

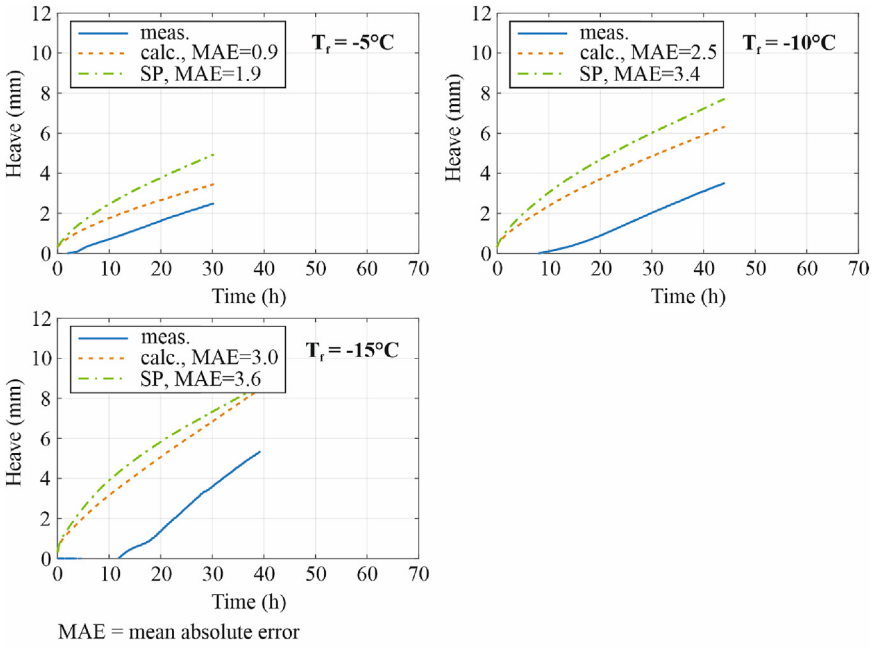

Fig. 18. Validation of semi-analytical approach for the thermal transient state under different temperature conditions for TF (soil 2).

7.1.1. Soil 1

A comparison of the new semi-analytical approach, the SP approach, and the measured values are shown in Fig. 17. The values of $C = 2.65 \times 10^{-5}$ cm^2/s and $SP = 3.3 \times 10^{-6}$ cm^2/(s °C) from Fig. 9 or Fig. 16, respectively, were used for the method's prediction. The tests used for validation have different cold side temperature boundary conditions between −5 °C and −17.5 °C (temperature gradient along the frozen soil part of ($\nabla T_f = 1\,°C\,/\mathrm{cm}$). There are two more tests with varying temperature gradients along the frozen soil part (Table 3). An overestimation of the total heave in both analytical approaches can explain the deviation between the calculated and measured values in Fig. 17 due to pore water expansion which is explained in Section 7.1 (TF: see Appendix A; Fig. A.6). The extra soil weight at BF that must be overcome during heaving leads to a poorer approximation than the TF results with no/less soil weight at the beginning of freezing. Generally, the overestimation of heaving occurs at the beginning of freezing which is attributed to an inaccurate calculation of the heave due to pore water expansion. Under natural conditions in partially saturated soils, 1D pore water expansion is not equivalent to heave at the surface, as water can also be expanded into air-filled pore spaces with no measurable effect at the surface. The slope between calculated and measured values becomes very similar after the first couple of freezing hours, indicating a good calculation of ice lens heaving during the thermal transient state.

The calculated heaving using the SP overestimates the measured data more than the approach presented here. This is attributed to the focus on the temperature gradient but not on the absolute flow length of the active area (for the relationship between thermal conditions and the unfrozen length, see Eq. (9)). For cases with very impermeable soil but a nearby water source (e.g. aquifer), the thickness of the unfrozen soil or flow path plays an important role. The results in Fig. 17 also show an apparent dependence of SP heaving on the temperature gradient. The heaving gradient increases with a larger temperature gradient (note that the temperature gradients of the first six cases with freezing temperatures between $-5\,°C \leq T_f \leq -17.5\,°C$ are equal at the end of transient freezing with $\nabla T_f = 1$ °C/cm, see Table 3). Compared to the SP approach, the new semi-analytical approach shows an improved performance of 14%, calculated by the mean absolute percentage error (MAPE) between the compared approaches of all tests.

7.1.2. Soil 2

Fig. 18 shows the approximation for soil 2 and TF tests under different temperatures T_f. As described in Section 7.1.1, the deviations between measured and calculated heaves are primarily caused by the determination of the pore water expansion. The mean saturation of soil 2 is lower than soil 1 (Table 2), which decreases heaving by water expansion into air-filled pores. Comparing the slope of the measured and calculated heaves, they run parallel over time, indicating a good approximation of the ice lens heave with the new approach. The SP approximation again shows less agreement with the measured data compared to the presented new approach. The new semi-analytical approach shows improved performance by 20%, calculated by MAPE between the compared approaches of all tests. The constants of the new approach and the SP for soil 2 are given with $C = 2.94 \times 10^{-5}$ cm^2/s and $SP = 4.22 \times 10^{-6}$ cm^2/(s °C).

7.2. Thermal quasi-steady state

For the calculation of frost heaving under different thermal boundary conditions for thermal quasi-steady state conditions, one frost heave test is used as a reference test for the calculation of the function $f(t)$ (Eq. (19)). The reference heave $h_{\mathrm{IL,Ref}}(t)$, e.g. measured by displacement transducer, and the unfrozen soil length l_{uf}, e.g. determined by temperature measurement, are used from this freezing test. Instead of l_{uf}, the thermal quotient $\Delta T_{\mathrm{uf}}/\nabla T_{\mathrm{uf}}$ can be determined by the warm side temperature boundary condition T_w (assuming 0 °C at the frost line) and the temperature gradient along the unfrozen part ∇T_{uf}, which is constant with time (for the relationship between thermal conditions and the unfrozen length see Eq. (9)).

The constant parameters a, b, c, and d of the functions $m(t)$ and $n(t)$ are calculated from at least two frost heave tests with different thermal boundary conditions (Eqs. (16)–(18)). As already

mentioned, no SP results are presented here as it is not applicable for this phase.

7.2.1. Soil 1

For the heave approximation of soil 1, a reference test with a freezing temperature of $T_f = -10$ °C was used. The reference test can be chosen arbitrarily as all functions $f(t)$ for different thermal boundary conditions coincide very well, as shown in Fig. 13. The parameters a, b, c and d were calculated in Section 5.2 (Figs. 11 and 12), and are given in Table 4.

Subsequently, the integral of $f(t)$ as a reference function can be calculated by Eq. (19). For the calculation of frost heaving under different thermal boundary conditions, only the warm temperature boundary condition T_w and the temperature gradient in the unfrozen soil ∇T_{uf} or the unfrozen soil length l_{uf} need to be known, e.g. from measurements or thermal calculations.

Fig. 19 shows the measured and calculated heave values over 150 h of freezing for different thermal boundary conditions. There are tests with different cold side temperature boundary conditions between −5 °C and −17.5 °C (temperature gradient along the frozen soil part of $\left(\nabla T_f = 1\,°C/cm\right)$ and two more tests with varying temperature gradient along the frozen soil part (Table 3), in accordance with the thermal transient tests. The results for the TF tests also fit very well (see Fig. A.7 in Appendix A).

Table 4
Calculated parameters for BF (soil 1).

Parameter	Value
a	0.0045
b	0.4654
c	1.3535
d	−0.1107

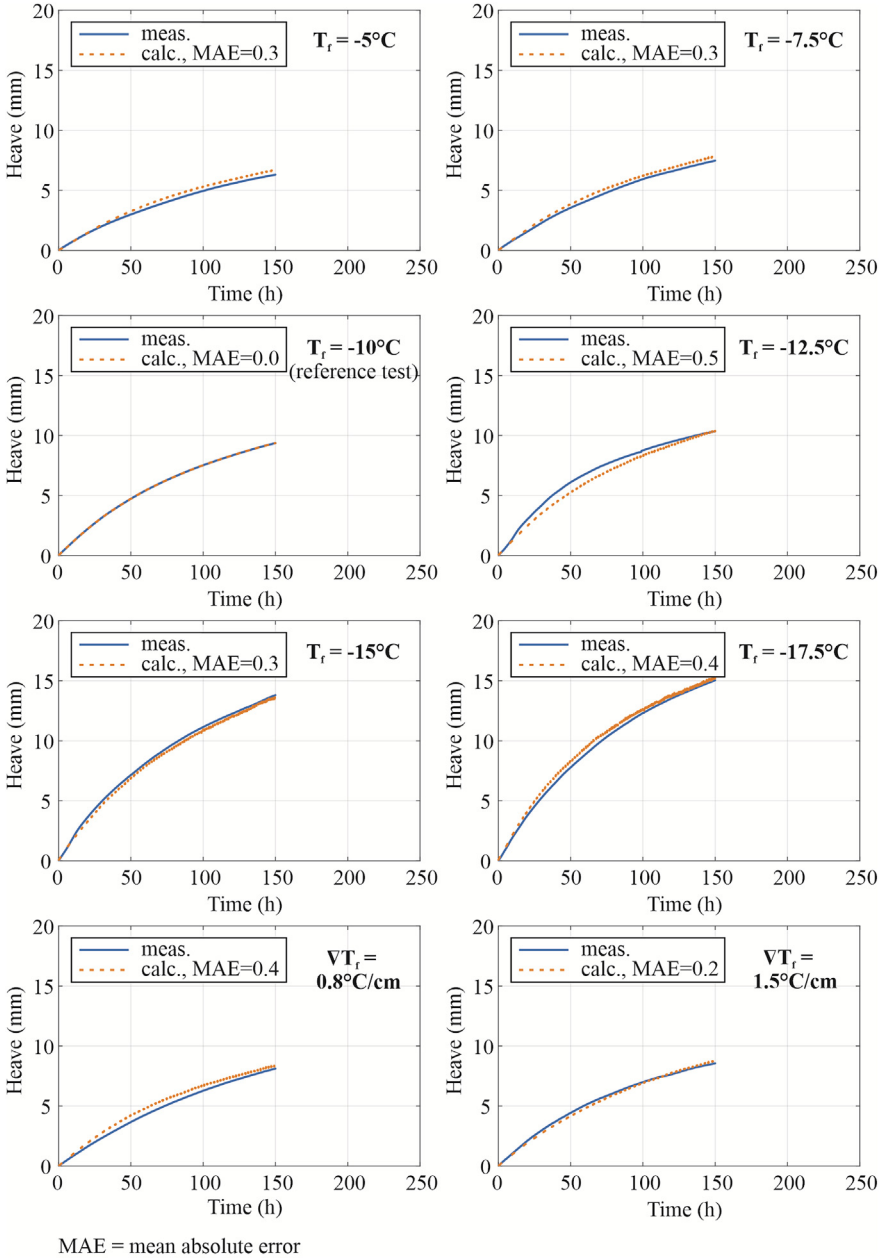

Fig. 19. Validation of semi-analytical approach for the thermal quasi-steady state under different temperature conditions for BF (soil 1).

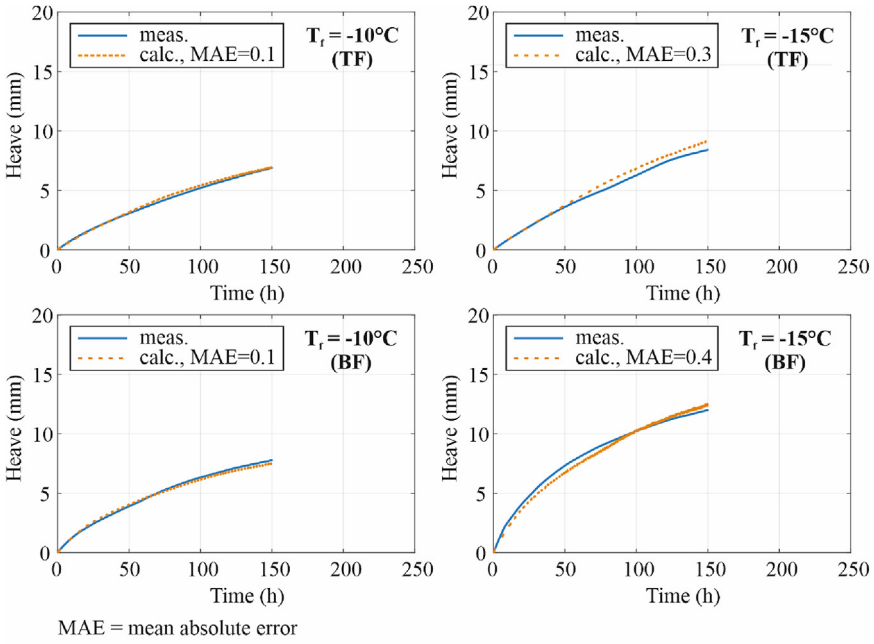

Fig. 20. Validation of semi-analytical approach for the thermal quasi-steady state under different temperature conditions for TF and BF (soil 2).

Table 5
Calculated parameters for TF and BF (soil 2).

Parameter	Value	
	TF	BF
a	0.0002	0.012
b	1.0721	0.4209
c	0.0956	1.2733
d	0.4254	−0.0131

7.2.2. Soil 2

Fig. 20 shows the measured and calculated ice lens heave of soil 2 for TF and BF and cold side boundary conditions of −10 °C and −15 °C. The function $f(t)$ was calculated using a reference test with a freezing temperature of −5 °C (arbitrarily selected). The values for *a*, *b*, *c* and *d* are given in Table 5.

8. Conclusions

The paper presents a semi-analytical approach calculating frost heaving due to ice lens formation. However, it does not only take into account typical conditions in AGF where the freezing direction is towards the ground surface (BF) with a layer of unfrozen soil above the frozen part as a flow path and relevant thermal conditions. We also include results for other freezing directions, mainly top-down freezing (TF), showing the method applies more generally.

The focus considers the thermal quasi-steady state, which only accounts for ice lens formation during a more extended freezing period. This state is comparable with the holding phase during AGF to preserve a specific frozen body thickness. This is important because the current SP method does not work during this stage.

Hence, the investigations were carried out for both the thermal transient and the thermal quasi-steady states. For thermal transient conditions, it was inferred that using the soil constant *C* is sufficient to calculate the ice lens heave of a particular soil for different thermal boundary conditions. The calculation of *C* only requires one frost heave test (1. FHT in Fig. 14). For thermal quasi-steady state, one additional test (2. FHT in Fig. 14) with a different freezing temperature as the 1. FHT is necessary to calculate the function $f(t)$. The function $f(t)$ is the same for one specific soil but under different thermal boundary conditions.

Experiments with two different soils validated the new semi-analytical approach under different thermal boundary conditions.

At the thermal transient state, the calculation of the pore water expansion is additionally required for the calculation of the total heave. The two test soils were not fully saturated, but the calculation did not consider water expansion into free pore spaces. Further, consolidation processes that occur primarily at BF due to the soil weight were neglected. This conservative calculation consequently slightly overestimates the measured heave. However, the slopes of the calculated heave curves correspond very well with the measured values with time which indicates a reliable ice lens calculation. The calculated SP results generally give a poorer agreement with the measured data. This especially applies when suction at the frost line occurs in very impermeable soil. For this case, the thickness of the unfrozen area (flow path to the ice lens) becomes relevant. Additionally, during thermal quasi-steady state conditions, the new calculation of the ice lens heave achieves an excellent agreement with the measured data for both soils.

The advantage of the semi-analytical approach is that only two frost heave tests are necessary to calculate ice lens heaving. No special soil testing is required since the calculated constant *C* for the thermal transient state or the function $f(t)$ for the thermal quasi-steady state includes the specific soil parameters which control the freezing suction and thus the water accumulation at the ice lens. Once *C* and $f(t)$ are known, frost heave with ice lens formation can be predicted for different thermal conditions.

Declaration of competing interest

The authors declare that they have no known competing financial interests or personal relationships that could have appeared to influence the work reported in this paper.

Acknowledgements

This work was supported by the German Research Foundation (DFG) under the project “Investigation and calculation of frost heave

considering specific boundary conditions of ground freezing" (Grant No. 409760547). The funding is herewith gratefully acknowledged. We also thank Prof. Em. Dr.-Ing. Martin Ziegler, former Professor of the chair of geotechnical engineering at RWTH Aachen University, provided insight and expertise that greatly assisted the research.

Appendix A. Supplementary data

Supplementary data to this article can be found online at https://doi.org/10.1016/j.jrmge.2023.07.004.

References

Arenson, L.U., Azmatch, T.F., Sego, D.C., Biggar, K.W., 2008. A new hypothesis on ice lens formation in frost-susceptible soils. In: Proceedings of the Ninth International Conference on Permafrost. Fairbanks, Alaska, pp. 59–64.
Arenson, L.U., Sego, D.C., 2006. The effect of salinity on the freezing of coarse-grained sands. Can. Geotech. J. 43 (3), 325–337.
Auld, F.A., Belton, J., Allenby, D., 2015. Application of artificial ground freezing. In: Proceedings of the XVI ECSMGE – Geotechnical Engineering for Infrastructure and Development, pp. 901–906. Edinburgh, United Kingdom.
Biermans, M.B.G.M., Dijkema, K.M., de Vries, D.A., 1978. Water movement in porous media towards an ice front. J. Hydrol. 37 (1–2), 137–148.
Black, P.B., 1995. Applications of the Clapeyron Equation to Water and Ice in Porous Media. US Army Corps of Engineers, Cold Regions Research & Engineering Laboratory Hanover, N.H.. CRREL report 95-6.
Busch, K., Luckner, L., Tiemer, K., 1993. Geohydraulik, third ed. Gebrüder Bornträger, Berlin, Germany.
Cai, H., Xu, L., Yang, Y., Li, L., 2018. Analytical solution and numerical simulation of the liquid nitrogen freezing-temperature field of a single pipe. AIP Adv. 8 (5), 055119.
Cai, H., Liu, Z., Li, S., Zheng, T., 2019. Improved analytical prediction of ground frost heave during tunnel construction using artificial ground freezing technique. Tunn. Undergr. Space Technol. 92, 103050.
Cai, H., Hong, R., Xu, L., Wang, C., Rong, C., 2022. Frost heave and thawing settlement of the ground after using a freeze-sealing pipe-roof method in the construction of the Gongbei Tunnel. Tunn. Undergr. Space Technol. 125, 104503.
Edlefsen, N., Anderson, A., 1943. Thermodynamics of soil moisture. Hilgardia 15 (2), 31–298.
Feng, Q., Fu, S., Wang, C., Liu, W., Wang, Y., Qiao, W., 2019. Analytical elasto-plastic solution for frost force of cold-region tunnels considering anisotropic frost heave in the surrounding rock. KSCE J. Civ. Eng. 23 (9), 3831–3842.
Fremond, M., Mikkola, M., 1991. Thermomechanical modelling of freezing soil. In: Yu, Wang (Eds.), International Symposium on Ground Freezing. Balkema, Rotterdam, Netherlands, pp. 17–24.
Gilpin, R.R., 1980. A model for the prediction of ice lensing and frost heave in soils. Water Resour. Res. 16 (5), 918–930.
Han, S.J., Goodings, D.J., 2006. Practical model of frost heave in clay. J. Geotech. Geoenviron. Eng. 132 (1), 92–101.
Hansson, K., Šimůnek, J., Mizoguchi, M., Lundin, L.C., Van Genuchten, M.T., 2004. Water flow and heat transport in frozen soil: numerical solution and freeze–thaw applications. Vadose Zone J. 3 (2), 693–704.
Hartge, K.H., 1978. Einführung in die Bodenphysik. Ferdinand Enke Verlag, Stuttgart, Germany.
Hartikainen, J., Mikkola, M., 1997. General thermomechanical model of freezing soil with numerical applications. In: Knutsson (Ed.), Ground Freezing 97, Frost Action in Soils. Balkema, Rotterdam, Netherlands, pp. 101–105.
Jessberger, H.L., Jagow, R., 1989. Determination of frost susceptibility of soils. Frost Geotech. Eng. 1, 449–469.
Ji, Y., Zhou, G., Zhou, Y., Vandeginste, V., 2019. Frost heave in freezing soils: a quasi-static model for ice lens growth. Cold Reg. Sci. Technol. 158, 10–17.
Jiang, B.S., Wang, J.G., Zhou, G.Q., 2009. Analytical calculation of temperature field around a single freezing pipe. J. China Univ. Min. Technol. 38 (4), 463–466.
Jin, H., Ryu, B.H., Lee, J., 2021. Engineering approach to determination of the Segregation Potential by the upward-step-freezing testing method. Cold Reg. Sci. Technol. 191, 103361.
Kaplar, C.W., 1970. Phenomenon and mechanism of frost heaving. Highw. Res. Rec. 304, 1–13.
Konrad, J.M., 1989. Pore water pressure at an ice lense: its measurement and interpretation. Cold Reg. Sci. Technol. 16 (1), 63–74.
Konrad, J.M., Morgenstern, N.R., 1980. A mechanistic theory of ice lens formation in fine-grained soils. Can. Geotech. J. 17 (4), 473–486.
Konrad, J.M., Morgenstern, N.R., 1981. The segregation potential of a freezing soil. Can. Geotech. J. 18 (4), 482–491.
Konrad, J.M., Morgenstern, N.R., 1982. Prediction of frost heave in the laboratory during transient freezing. Can. Geotech. J. 19 (3), 250–259.
Konrad, J.M., Shen, M., 1996. 2-D frost action modeling using the segregation potential of soils. Cold Reg. Sci. Technol. 24 (3), 263–278.
Kutílek, M., 1972. Non-darcian flow of water in soils-laminar region: a review. Dev. Soil Sci. 2, 327–340.
Li, T., Zhou, Y., Shi, X.Y., Hu, X.X., Zhou, G.Q., 2018. Analytical solution for the soil freezing process induced by an infinite line sink. Int. J. Therm. Sci. 127, 232–241.
Loch, J.P.G., 1978. Thermodynamic equilibrium between ice and water in porous media. Soil Sci. 126 (2), 77–80.
Lyu, Z., Xia, C., Liu, W., 2020. Analytical solution of frost heaving force and stress distribution in cold region tunnels under non-axisymmetric stress and transversely isotropic frost heave of surrounding rock. Cold Reg. Sci. Technol. 178, 103117.
Ma, W., Zhang, L., Yang, C., 2015. Discussion of the applicability of the generalized Clausius–Clapeyron equation and the frozen fringe process. Earth Sci. Rev. 142, 47–59.
Michalowski, R.L., Zhu, M., 2006. Frost heave modelling using porosity rate function. Int. J. Numer. Anal. Methods GeoMech. 30 (8), 703–722.
Miller, R.J., Low, P.F., 1963. Threshold gradient for water flow in clay systems. Soil Sci. Soc. Am. J. 27 (6), 605–609.
Niggemann, K., Ziegler, M., Fuentes, R., 2023. Influence of freezing directions on ice lens formations in soils. Preprint at engrxiv. https://doi.org/10.31224/3129.
Nishimura, S., Gens, A., Olivella, S., Jardine, R.J., 2009. THM-coupled finite element analysis of frozen soil: formulation and application. Geotechnique 59 (3), 159–171.
Nixon, J.F., 1982. Field frost heave predictions using the segregation potential concept. Can. Geotech. J. 19 (4), 526–529.
Nixon, J.F., 1991. Discrete ice lens theory for frost heave in soils. Can. Geotech. J. 28 (6), 843–859.
O'Neill, K., Miller, R.D., 1982. Numerical Solutions for a Rigid-Ice Model of Secondary Frost Heave. US Army Corps of Engineers, Cold Regions Research & Engineering Laboratory Hanover, N.H.. CRREL report 18-13.
O'Neill, K., Miller, R.D., 1985. Exploration of a rigid ice model of frost heave. Water Resour. Res. 21 (3), 281–296.
Penner, E., 1986. Aspects of ice lens growth in soils. Cold Reg. Sci. Technol. 13 (1), 91–100.
Rempel, A.W., 2007. Formation of ice lenses and frost heave. J. Geophys. Res.: Earth Surf. 112 (F2), 1–17.
Rempel, A.W., 2010. Frost heave. J. Glaciol. 56 (200), 1122–1128.
Sheng, D., Axelsson, K., Knutsson, S., 1995. Frost heave due to ice lens formation in freezing soils: 1. Theory and verification. Nord. Hydrol 26 (2), 125–146.
Suh, H.S., Sun, W., 2022. Multi-phase-field microporomechanics model for simulating ice-lens growth in frozen soil. Int. J. Numer. Anal. Methods GeoMech. 46 (12), 2307–2336.
Sweidan, A., Niggemann, K., Heider, Y., Ziegler, M., Markert, B., 2021. Experimental study and numerical modeling of the thermo-hydro-mechanical processes in soil freezing with different frost penetration directions. Acta Geotech 17 (1), 231–255.
Tiedje, E., Guo, P., 2012. Frost heave modeling using a modified segregation potential approach. In: Cold Regions Engineering 2012: Sustainable Infrastructure Development in a Changing Cold Environment, pp. 686–696.
von Soos, P., Engel, J., 2017. Eigenschaften von Boden und Fels–ihre Ermittlung im Labor. In: Karl Josef Witt (Ed.), Grundbau-Taschenbuch: Teil 1: Geotechnische Grundlagen. Ernst & Sohn, Berlin, Germany, pp. 139–242.
Wang, Z., Shen, L., Xie, J., 2014. Study on temperature field variation of the surrounding soil mass caused by artificial single pipeline freezing. Mod. Tunn. Technol. 54 (1), 110–116.
Wilen, L.A., Dash, J.G., 1995. Frost heave dynamics at a single crystal interface. Phys. Rev. Lett. 74 (25), 5076–5079.
Xia, D., Arenson, L.U., Biggar, K.W., Sego, D.C., 2005. Freezing process in Devon silt-using time-lapse photography. In: Proceedings of the 58th Canadian Geotechnical Conference, Saskatoon, Saskatchewan. Canada.
Zhao, X., Yang, X., Zhang, H., Lai, H., Wang, X., 2020. An analytical solution for frost heave force by the multifactor of coupled heat and moisture transfer in cold-region tunnels. Cold Reg. Sci. Technol. 175, 103077.
Zhang, L., Ma, W., Yang, C., Wen, Z., Dong, S., 2016. An investigation of pore water pressure and consolidation phenomenon in the unfrozen zone during soil freezing. Cold Reg. Sci. Technol. 130, 21–32.
Zhang, X., Sheng, Y., Huang, L., Huang, X., He, B., 2020. Application of the segregation potential model to freezing soil in a closed system. Water 12 (9), 2418.
Zhang, Y., Michalowski, R.L., 2015. Thermal-hydro-mechanical analysis of frost heave and thaw settlement. J. Geotech. Geoenviron. Eng. 141 (7), 04015027.
Zhu, Y., Li, Y., Hao, Z., Luo, L., Luo, J., Wang, L., 2021. An analytical solution for the frost heaving force and displacement of a noncircular tunnel. Comput. Geotech. 133, 104022.



Katharina Niggemann obtained her BSc and MSc degrees in construction engineering with a major in geotechnical engineering and tunnel construction from RWTH Aachen University, Germany, in 2012 and 2015, respectively. She was affiliated as scientific staff at the Institute of Geomechanics and Underground Technology of RWTH Aachen University from 2015 to 2022. Her research interests include (1) experimental investigations on frost heave with ice lens formation in fine-grained soils; and (2) theoretical study on frost heave calculation during artificial ground freezing. For her research, she has been participated on a project funded by the German Research Foundation (DFG).